Rapid Communications

Origin of planar Hall effect on the surface of topological insulators: Tilt of Dirac cone by an in-plane magnetic field

Shi-Han Zheng,[1,2] Hou-Jian Duan,[1] Jia-Kun Wang,[1] Jia-Yu Li,[1] Ming-Xun Deng,[1,*] and Rui-Qiang Wang[1,†]

[1]*Guangdong Provincial Key Laboratory of Quantum Engineering and Quantum Materials, SPTE, South China Normal University, Guangzhou 510006, China*

[2]*College of Automation, Zhongkai University of Agriculture and Engineering, Guangzhou 510225, China*

(Received 14 September 2019; revised manuscript received 28 November 2019; published 21 January 2020)

Recently, a novel planar Hall effect (PHE), which results from the resistivity anisotropy induced by an in-plane magnetic field, was discovered on the surface of topological insulators (TIs). While the PHE phenomenon in Weyl/Dirac semimetals is understood as a consequence of the chiral anomaly, the origin of the PHE in TIs, however, remains unclear theoretically. Several theories and experiments have ascribed the appearance of the PHE to the anisotropic backscattering induced by magnetic disorders, where the magnetization of the scatterers is indispensable. Instead, we here show that the anisotropic backscattering can arise from the tilt of the Dirac cone by an in-plane magnetic field, which emerges if nonlinear momentum terms are included, irrelevant to the magnetic nature of the scatterers. We further find that a relatively strong scalar potential can further enhance the PHE magnitude significantly, and the resulting impurity resonant state together with the tilted cone can produce the double-peak structure of the PHE and the sign change of the anisotropic magnetoresistivity. Our theory provides another perspective to understand the nontopological origin of the experimentally observed PHE in topological materials.

DOI: 10.1103/PhysRevB.101.041408

Introduction. Magnetotransport measurement is an extremely powerful and experimentally reliable tool to explore the properties of materials. Recently, the negative longitudinal magnetoresistivity (LMR) in the presence of parallel magnetic and electric fields has been confirmed experimentally in a series of newly discovered topological semimetals and is widely believed to be a signature of the chiral anomaly [1–11]. Nevertheless, this explanation becomes ambiguous since the negative LMR also emerges in other systems where the chiral anomaly is not well defined, e.g., in topological insulators [12–15]. Recent theories addressed that the chiral anomaly in Dirac and Weyl semimetals [16–18] can induce another intriguing effect, planar Hall effect (PHE), which has been probed in quite a few experiments [19–23]. The PHE, usually occurring in ferromagnetic systems [24–26], manifests itself as a detectable transverse voltage in response to a magnetic field applied in the plane of the sample and electric current. The combination of the PHE with the negative LMR is proposed to be a key transport signature of the chiral anomaly [16], which also interpreted the angle narrowing of LMR oscillation with magnetic field direction, observed in recent experiment [1].

Interestingly, the PHE has also been reported recently in doped three-dimensional topological insulators (TIs) [27–29]. While the PHE phenomenon in Dirac/Weyl semimetals was well understood with the chiral anomaly, the origin of the PHE in TIs still remains unclear theoretically. In a very recent experiment [27], Taskin *et al.* observed the PHE on a TI $Bi_{2-x}Sb_xTe_3$ sample doped with nonmagnetic impurities, which is contributed by the spin-momentum locking surface states of the TIs. Afterwards, Shubnikov–de Haas oscillations [28] of the PHE were observed in Sn-doped $Bi_{1.1}Sb_{0.9}Te_2$, further evidencing the PHE originating from the topological surface states. To explain such PHE, Taskin *et al.* employed a theory model of electron scattering off magnetic impurities polarized by an in-plane magnetic field, in the spirit of the existing theories [30,31] in which the magnetization of impurity is indispensable. As addressed in Ref. [27], while their model is not expected to give a microscopic description of the actual disorder in the experiment, it is a minimal model capturing the field-induced anisotropic scattering essential to explain the experiment. Also, to explain the simultaneously observed sign change of the in-plane anisotropic magnetoresistivity (AMR) and the unequal oscillating amplitudes between the AMR and PHE, they took into account a possible extra out-of-plane magnetic field. The sign change of the AMR has been reported by Sulaev *et al.* in first-principles calculations [32] and ascribed to the in-plane magnetic-field-induced shift of two coupled surface states. Akzyanov *et al.* [33] took the effect of hexagonal warping of TI surface states into account and obtained the angle dependence of transverse conductivity σ_{xy} following the function $\cos(3\theta)$, different from the experimentally observed result of $\cos\theta\sin\theta$, where θ is the relative angle between the magnetic field and current directions. Nandy *et al.* [34] addressed that the nontrivial Berry phase and magnetic moments of bulk states may act as an origin of planar Hall response, but obviously it cannot be applicable to the above experiments with respect to TI surface states.

*dengmingxun@scnu.edu.cn
†wangruiqiang@m.scnu.edu.cn

In this Rapid Communication, we propose a microscopic mechanism as an origin of the observed PHE and in-plane AMR on the surface of TIs [27,28], namely, the tilt of the Dirac cone induced by the applied in-plane field itself in measurement of magnetoresistivity, not requiring magnetic nature of the scatterers. In the TIs with nonlinear momentum terms, e.g., describing the asymmetry between the electron and hole bands, an in-plane magnetic field can tilt the upright Dirac cone due to the broken Lorentz invariance. We find that the tilted band structure can generate the PHE. Further consideration of electron scattering off a strong impurity potential can simultaneously produce the two-peak structure of PHE, sign change of the in-plane AMR, and unequal oscillating amplitudes between the AMR and PHE, all of which were observed experimentally [27], with no need to introduce other extra mechanisms.

Model and Hamiltonian. We consider an experimental model with the low-energy Dirac electrons on the helical surface of TIs coupled to pointlike nonmagnetic impurities, which are randomly distributed at position $\mathbf{r}_n$ and read $V_{im}(\mathbf{r}) = \sum_n U\delta(\mathbf{r}-\mathbf{r}_n)$ with a scalar potential U. The Hamiltonian of the TI is described by $H_{TI} = \sum_{\mathbf{k}'\sigma\sigma'} c^\dagger_{\mathbf{k}'\sigma} h_{TI}(\mathbf{k}')_{\sigma\sigma'} c_{\mathbf{k}'\sigma'}$, with $h_{TI}(\mathbf{k}') = \varepsilon_0(\mathbf{k}') + \hbar v_F(\mathbf{k}'\times\sigma)_z - \sigma\cdot\mathbf{B}_\parallel - \mu$. Here, $c^\dagger_{\mathbf{k}'s} = (c^\dagger_{\mathbf{k}'\uparrow}, c^\dagger_{\mathbf{k}'\downarrow})$ is the creation operator of electrons with wave vector $\mathbf{k}' = (k'_x, k'_y)$, v_F represents the Fermi velocity, σ is the spin Pauli matrices, and μ is the electrochemical potential. The nonlinear momentum terms $\varepsilon_0(\mathbf{k}')$ in TIs can stem from the asymmetry between the electron and hole bands or the hexagonal warping effect. For simplicity, we here only consider the particle-hole asymmetry [35–37] with $\varepsilon_0(\mathbf{k}') = D\mathbf{k}'^2$. With respect to the PHE, we would concentrate on the influence of an in-plane magnetic field $\mathbf{B}_\parallel = (B_x, B_y) = B(\cos\theta_B, \sin\theta_B)$. If only taking the linear TI dispersion $\varepsilon_0(\mathbf{k}') = 0$, $\mathbf{B}_\parallel$ can be gauged out and so has no effect on the PHE. However, this is not the case for finite $\varepsilon_0(\mathbf{k}')$, since $\mathbf{B}_\parallel$ not only shifts the origin point of the Dirac cone $(0,0) \to (B_y, -B_x)/\hbar v_F$ but also leads to tilt of the Dirac cone. This point can be clearly seen when one expands the Hamiltonian around the shifted Dirac point $(B_y, -B_x)/\hbar v_F$, which is given by

$$h_{TI}(\mathbf{k}) = \varepsilon_0(\mathbf{k}) + \hbar v_F(\mathbf{k}\times\sigma)_z + \hbar v_B(k_x\sin\theta_B - k_y\cos\theta_B) - \mu, \tag{1}$$

where $\hbar v_B = 2DB/\hbar v_F$ and the constant $\mathbf{B}^2_\parallel$ is dropped. Obviously, the third term tilts the pristine upright Dirac cone, as compared in Figs. 1(a) and 1(b). The intrinsic tilted dispersion of the Dirac cone also exists in two-dimensional Dirac semimetals with special crystal symmetries [38,39]. In contrast, the tilted dispersion here is induced by the external field and so exhibits a strong dependence on $\mathbf{B}_\parallel$. The tilted effect can be ignored in discussion of the out-plane magnetoresistivity but it will play a decisive role for the PHE. After introduction of the tilted term, for convenience of analytical calculations, we first set $\varepsilon_0(\mathbf{k}) = 0$. In the above treatment, we also have chosen the gauge for the vector potential $\mathbf{A} = (0, 0, A_z)$ and therefore the orbital effect can be ignored. In the following, we find that this field-induced anisotropic energy dispersion will lead to the PHE even though the Dirac electrons are scattered off nonmagnetic impurities.

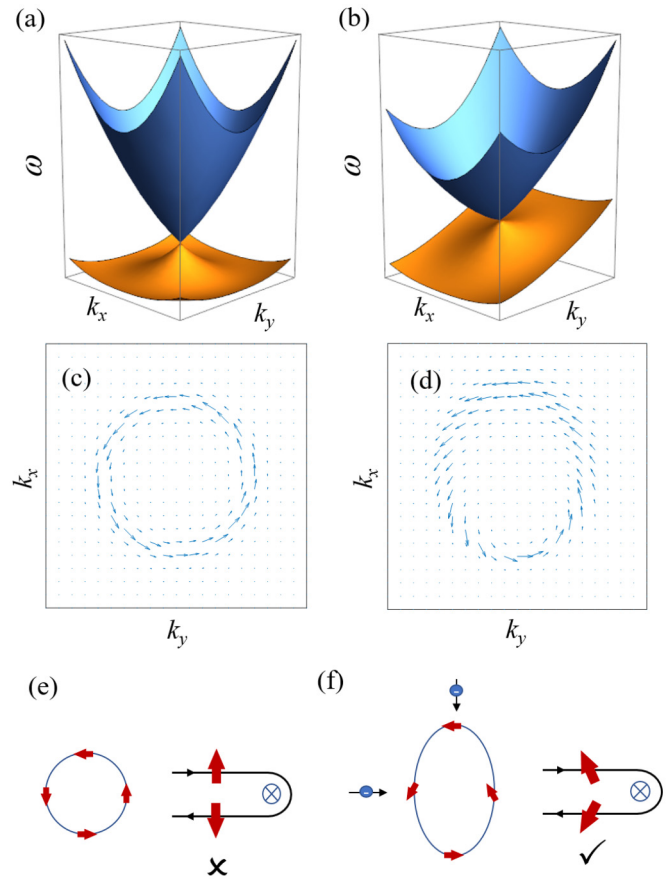

FIG. 1. (a),(b) The Dirac energy band, (c),(d) spin texture at the Fermi contour, and (e),(f) schematic picture of electron scattering off nonmagnetic impurities, for TI surface states with hole-particle asymmetry $\varepsilon_0(\mathbf{k}) = D\mathbf{k}^2$. Left panels: without tilt; right panels: with tilt by an in-plane magnetic field. In (f), the prohibition of spin-flip backscattering between states $|\mathbf{k}\rangle$ and $|-\mathbf{k}\rangle$ is lifted along the magnetic field (i.e., horizontal) direction when scattering off a scalar potential, because the spins $\mathbf{s}_\mathbf{k}$ and $\mathbf{s}_{-\mathbf{k}}$ are not orthogonal at the elliptic Fermi surface. In (e) and (f), the red and black arrows stand for the spin and momentum direction of a Dirac electron, respectively.

Band tilt-induced PHE. We use the Streda-Smrcka version [40–42] of the Kubo formula to calculate the conductivity

$$\sigma_{ij} = -\frac{e^2}{2h}\int d\omega \frac{\partial f(\omega)}{\partial\omega}\sum_{\mathbf{k}} \mathrm{Tr}\big\{v_i[G^r(\mathbf{k},\omega) - G^a(\mathbf{k},\omega)] \times v_j G^a(\mathbf{k},\omega) - v_i G^r(\mathbf{k},\omega) v_j[G^r(\mathbf{k},\omega) - G^a(\mathbf{k},\omega)]\big\}, \tag{2}$$

where $v_i = \partial h_{TI}/\partial k_i$ is the velocity operator, $f(x) = [e^{(x-\mu)/k_BT} + 1]^{-1}$ is the Fermi distribution function, and the retarded/advanced Green's functions $G^{r/a}(\mathbf{k},\omega)$ are obtained as

$$G^{r/a}(\mathbf{k},\omega) = \frac{1}{2}\sum_{\gamma=\pm}[1 + \gamma\mathbf{n}_\mathbf{k}\cdot\sigma]G^{r/a}_\gamma(\mathbf{k},\omega). \tag{3}$$

Here, we define a momentum unit vector $\mathbf{n}_\mathbf{k} = (-k_y, k_x, 0)/|\mathbf{k}|$ and band-dependent Green's functions $G^{r/a}_\gamma(\mathbf{k},\omega) = [\omega + \mu \pm i\Gamma - E_{\mathbf{k}\gamma}]^{-1}$ with the energy

$E_{\mathbf{k}\gamma} = \hbar v_B(k_x \sin\theta_B - k_y \cos\theta_B) + \gamma \hbar v_F|\mathbf{k}|$ for the conduction band ($\gamma = +$) and valence band ($\gamma = -$). To see the influence of the reshaped band, we first consider the weak scalar potential by introducing a constant self-energy $i\Gamma$.

At zero temperature, $T \to 0$, after performing the integral and summation in Eq. (2), we obtain σ_{ij} (detailed derivations are given in the Supplemental Material [43]):

$$\sigma_{xx} = \sigma_\perp + (\sigma_\parallel - \sigma_\perp)\cos^2\theta_B,$$
$$\sigma_{xy} = (\sigma_\parallel - \sigma_\perp)\sin\theta_B\cos\theta_B, \tag{4}$$

with $\sigma_\perp = \frac{1}{2}\frac{e^2}{h}\frac{|\mu|}{\Gamma}$ and $\sigma_\parallel = \frac{e^2}{h}\frac{|\mu|}{\Gamma}(\frac{1}{2} - \frac{v_B^2}{v_F^2})$ for a not too strong magnetic field $\hbar v_B \ll \hbar v_F$. Obviously, the interesting PHE σ_{xy} emerges and shows a nonzero value for all field directions except for the parallel and perpendicular orientations. σ_{xy} and σ_{xx} satisfy the typical behaviors. Different from the ordinary Hall effect which satisfies the antisymmetry property, the PHE σ_{xy} is symmetric with respect to the magnetic field since it is not generated by the conventional Lorentz force. It is emphasized that the appearance of this PHE does not originate from spin polarization of impurities as proposed in Refs. [27,30,31].

We can understand the raised PHE as follows. The spin-flip scattering is a necessary condition to cause the transverse PHE. Without tilt, $E_{\mathbf{k}\gamma}$ is independent of direction angle θ_k of $\mathbf{k}$, and after integral over θ_k, the spin-flip (off-diagonal) term $\mathbf{n}_{\mathbf{k}\gamma}\cdot\sigma$ vanishes. However, finite tilt makes $E_{\mathbf{k}\gamma}$ depend on $B_x k_y - B_y k_x$ and so the integration over θ_k cannot cancel the spin-flip term. Physically, the prohibition of backscattering between states $|\mathbf{k}\rangle$ and $|-\mathbf{k}\rangle$ is lifted along the field direction because their spins $\mathbf{s}_\mathbf{k}$ and $\mathbf{s}_{-\mathbf{k}}$ are not orthogonal due to the elliptic Fermi surface, as illustrated in Figs. 1(d) and 1(f). But, it is not the case along the direction perpendicular to the magnetic field. This point can be easily verified by calculating $\mathbf{s}_\mathbf{k} = \langle\sigma_\mathbf{k}\rangle$ with the eigenstates of Hamiltonian Eq. (1). As a consequence of the anisotropy of scattering, there emerges above PHE and AMR. Even though the scattering potential is isotropic, the electron scattering still explicitly depends on the direction of both incident and scattered electrons' waves. This scenario is very different from that in previous theories [30,31], where the spin flip originates from scattering off magnetic impurities.

Nonmagnetic impurity enhanced PHE. The above discussions focus on the case of weak impurity potential. For a strong impurity potential, we can obtain the impurity averaged Green's function of surface states from the Dyson equation

$$G(\mathbf{k}, i\omega_n) = G_0(\mathbf{k}, i\omega_n)[1 - \Sigma(i\omega_n)G_{\mathbf{k}0}(\mathbf{k}, i\omega_n)]^{-1}, \tag{5}$$

where $G_0(\mathbf{k}, i\omega_n) = 1/[i\omega_n - h_{TI}(\mathbf{k})]$ is the bare Green's function of the undisturbed TI surface and the impurity effect is taken into account by the self-energy $\Sigma(i\omega_n)$. In the Born approximation up to the first order in impurity concentration n_i, we can calculate the self-energy by using the T-matrix approach [44–46], $\Sigma(i\omega_n) = n_i[\sigma_0 - U g(i\omega_n)]^{-1}U$, where $g(i\omega_n) = \sum_\mathbf{k} G_0(\mathbf{k}, i\omega_n)$. As a consequence, we find that the impurity averaged Green's function also have the same expression as Eq. (3) only if replacing the momentum $\mathbf{k}$ with $\tilde{\mathbf{k}} = (k_x + \Sigma_y/\hbar v_F, k_y - \Sigma_x/\hbar v_F)$ and $i\Gamma$ with Σ_0, where we denote $\Sigma(i\omega_n) = \Sigma_0\sigma_0 + \sum_{j=x,y}\Sigma_j\sigma_j$.

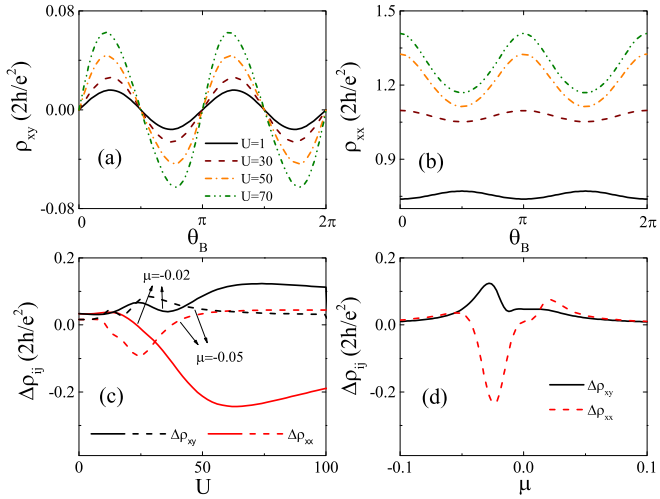

FIG. 2. Variation of (a) PHR ρ_{xy} and (b) AMR ρ_{xx} with direction θ_B of the magnetic field for $\mu = -0.02$ and impurity potential $U = 1, 30, 50, 70$. (c) The oscillating amplitudes $\Delta\rho_{xy}$ of PHE and $\Delta\rho_{xy}$ of AMR as a function of U for different chemical potentials $\mu = -0.02$ and -0.05. (d) $\Delta\rho_{xy}$ and $\Delta\rho_{xx}$ as a function of μ for $U = 50$. The impurity concentration is fixed at $n_i = 0.05\%$ and other parameters are chosen as $D = 0.5$, $\hbar v_B = 0.3$, $\hbar v_F = 1$, and all the energies are measured in a unit of the cutoff energy $\Lambda = 1$.

We carry out numerical calculations for planar Hall resistivity (PHR) $\rho_{xy} = \sigma_{xy}/(\sigma_{xx}^2 + \sigma_{xy}^2)$ and AMR $\rho_{xx} = \sigma_{xx}/(\sigma_{xx}^2 + \sigma_{xy}^2)$. In the numerical calculations, we also pick up the quadratic term $\varepsilon_0(\mathbf{k}) = D\mathbf{k}^2$. In Figs. 2(a) and 2(b), we plot the PHR ρ_{xy} and AMR ρ_{xx} as a function of direction θ_B of magnetic field. Obviously, for weak impurity potential $U = 1$, ρ_{xy} and ρ_{xx} follow Eq. (4), i.e., exhibiting the $\sin\theta_B\cos\theta_B$ and $\cos^2\theta_B$ angular dependence, respectively. Moreover, the oscillating amplitude $\Delta\rho_{xy} = \rho_{xy}(\theta_B = \pi/4)$ of the PHR is strictly equal to $\Delta\rho_{xx} = \frac{1}{2}[\rho_{xx}(\theta_B = \pi/2) - \rho_{xx}(\theta_B = 0)]$ of the AMR. With enhancement in the impurity potential, while the typical angle dependences, ρ_{xy} on $\sin\theta_B\cos\theta_B$ and ρ_{xx} on $\cos^2\theta_B$, do not change, ρ_{xx} and ρ_{xy} present different oscillating amplitudes. These unequal amplitudes are contributed by the off-diagonal components Σ_x and Σ_y of the self-energy, which instead approximately vanish for the weak impurity potential. In order to clarify this point, we derive analytical expressions for conductivities by considering a little stronger potential. When keeping Σ_x and Σ_y to the leading order and ignoring the quadratic term $\varepsilon_0(\mathbf{k})$, we find that the longitudinal and transverse conductivities in Eq. (4) are corrected by an extra part (seeing the detailed derivation in the Supplemental Material [43]):

$$\sigma_{xx}^{ex} = \tfrac{5}{4}\xi - \tfrac{3}{2}\xi\cos^2\theta_B,$$
$$\sigma_{xy}^{ex} = -\tfrac{5}{4}\xi\sin\theta_B\cos\theta_B, \tag{6}$$

where $\xi = \mathrm{sgn}(\mu)\frac{\zeta_-(\mu^+)+\zeta_-(\mu^-)}{\Gamma}\frac{v_B}{v_F}\frac{e^2}{h}$ with $\zeta_-(\mu)$ the angle-independent part of the self-energies Σ_x and Σ_y. As seen from Eq. (6), while the correction by the off-diagonal components of the self-energy presents the same angle dependence as Eq. (4), it, indeed, makes the oscillating amplitude unequal.

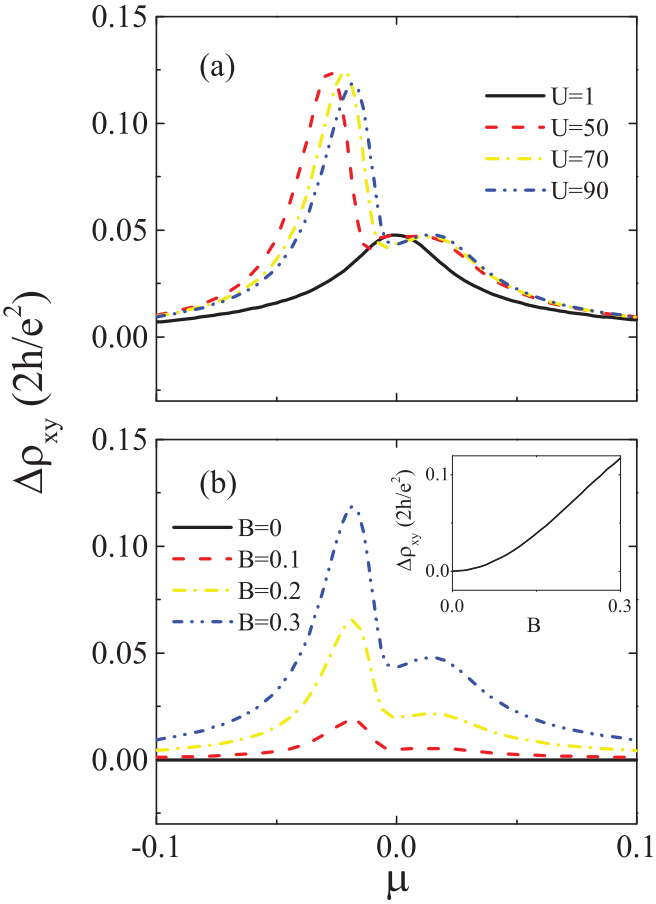

FIG. 3. Evolution of the double-peak structure in PHR amplitude $\Delta\rho_{xy}$ with (a) different U and fixed $B = 0.3$, and (b) different B and fixed $U = 90$, as a function of chemical potential μ (tunable by a gate voltage). The inset of (b) shows the peak in $\Delta\rho_{xy}$ as a function of the magnetic field strength B for $\mu = -0.02$. The other parameters are the same as in Fig. 2.

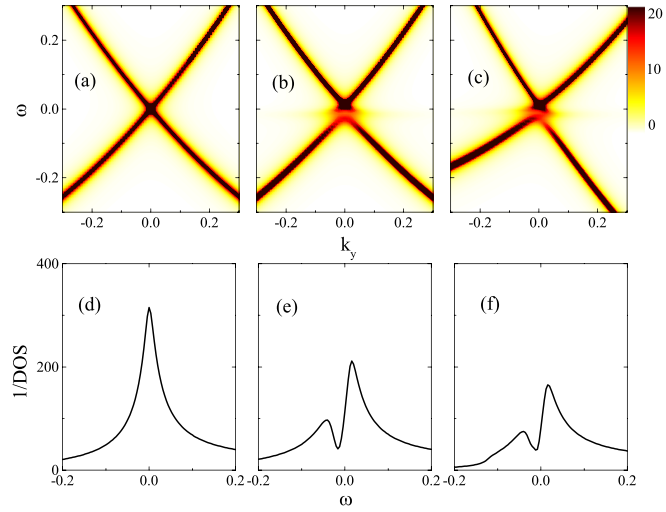

FIG. 4. The energy dispersion of helical surface states in TIs with (a) $U = 1$ and $B = 0$, (b) $U = 90$ and $B = 0$, and (c) $U = 90$ and $B = 0.3$. (d)–(f) The reversed density of states (1/DOS) corresponding to (a)–(c), respectively. Impurity-induced resonant states are developed remarkably in (b) and (c) for large U. The other parameters are the same as in Fig. 2.

In Figs. 2(c) and 2(d), we depict the oscillating amplitudes as a function of U and electrochemical potential μ, respectively. With the increase of U or μ, while the amplitude $\Delta\rho_{xy}$ of the PHR never changes the sign, the amplitude $\Delta\rho_{xx}$ of the AMR changes from positive to negative value, whose threshold is related to μ in Fig. 2(c) and U in Fig. 2(d). The unequal oscillating amplitudes between the AMR and PHR and the sign change of AMR have been observed in recent experiments [27], the origin of which was attributed to the orbital magnetoresistance induced by an out-of-plane magnetic field due to a possible misalignment of the rotation plane with respect to the film plane; very different from the present mechanism of the strong impurity potential. In fact, the strong impurity potential plays a role through impurity resonant states as addressed below.

In Figs. 3(a) and 3(b) we illustrate the dependence of the PHR amplitude $\Delta\rho_{xy}$ on U and B, respectively, as a function of chemical potential μ which is tunable by a gate voltage in experiments. Interestingly, Fig. 3 presents a double-peak structure near the Dirac point, reproducing the scenario in the experiment [27]. From Fig. 3(a), one can see that two peaks are formed for strong impurity potential U. Otherwise, only one peak emerges for weak impurity potential $U = 1$. Figure 3(b) shows the dependence of peaks on B. Obviously, the double-peak structure is sensitive to B, which reduces as a whole with B decreasing. The PHE vanishes completely for $B = 0$ even for strong impurity potential because the spin-flip scattering is prohibited by the spin-momentum locking of helical Dirac electrons. In the inset of Fig. 3(b), a quadraticlike dependence of $\Delta\rho_{xy}$ on B is shown for small B and linearlike dependence for large B. In order to clarify the origin of the double-peak structure in ρ_{xy}, we plot the spectrum function $A(\mathbf{k}, \omega) = -\frac{1}{\pi}\,\mathrm{Im}[\mathrm{Tr}G(\mathbf{k}, i\omega_n \to \omega + i0^+)]$ in Figs. 4(a)–4(c), which characterizes the energy dispersion of TI surface states, and the corresponding reversed density of state $1/\mathrm{DOS} = 1/\sum_{\mathbf{k}} A(\mathbf{k}, \omega)$ in Figs. 4(d)–4(f). For weak impurity potential $U = 1$ in Fig. 4(a), the approximate typical linear dispersion appears and correspondingly, 1/DOS in Fig. 4(d) shows a single-peak structure due to vanished DOS in the Dirac point $\omega = 0$. With the increase in U, the dispersion becomes fuzzy in the vicinity of the Dirac point, as shown in Fig. 4(b), where an impurity resonant state develops. The impurity resonant state exhibits a peak in DOS or a dip in 1/DOS, around which two peaks emerge in both sides, as shown in Fig. 4(e). The PHR is proportional to 1/DOS [43] and so the double-peak structure in ρ_{xy} originates from the impurity resonant state. Actually, the impurity resonance peaks have been extensively reported in many theories and experiments [44–47]. The resonant-peak position ω_c is determined by the singular point of $\Sigma(i\omega_n)$, i.e., $\mathrm{Re}[1 - 2Ug_0 + U^2g_0^2 - U^2g_1^2] = 0$ where g_0 and g_1 are diagonal and off-diagonal matrix elements of Green's function $g(i\omega_n)$ in spin space. As $\mathbf{B}_\parallel$ is introduced, it is natural that the resonant magnitude and position are dependent on B through g_1, as depicted in Figs. 4(c) and 4(f). Physically, resonant states delay the electron lifetime located at the impurity and so enhance the resistivity. The strong energy and spin dependence of self-energies in the resonant state contribute

differently to σ_{xx} and σ_{xy} in Eq. (2), which in turn leads to different behaviors between the oscillating amplitudes of the AMR and PHR.

In our Rapid Communication, we used dimensionless units by setting $\hbar v_F = 1$ and the cutoff energy $\Lambda = \hbar v_F k_c = 1$ of the energy band for convenience of analysis. In practice, the impurity potential U and chemical potential μ possess the dimension of energy, which are scaled by the cutoff energy Λ, and parameter D is scaled by $(\Lambda/\hbar v_F)^2$. In the three-dimensional topological insulators Bi_2Se_3 [47], the cutoff energy is $\Lambda = 300$ meV and the Fermi velocity is $v_F \simeq 5 \times 10^5$ m/s. According to this, we estimate the parameters in our Rapid Communication as follows: the chemical potentials plotted in the range $\mu \in (-0.1, 0.1)$ correspond to $(-30, 30)$ eV, $U = 90$ corresponds to about 27 eV, which are available experimentally, for example in experiment [47] where $U = 45$ eV, and $D = 0.5$ stands for $D \approx 15$ eV Å^2, which is within the range of realistic topological insulator samples [48].

Conclusion and remarks. In conclusion, we have proposed a microscopic mechanism to explain the experimentally observed PHE on the surface of TIs. We find that the Dirac cone with nonlinear momentum terms can be tilted by an in-plane magnetic field and the resulting anisotropic backscattering leads to the PHE, in stark contrast to previous theories. When considering the Dirac electrons scattering off a strong scalar potential, the emerging impurity resonant state together with the tilted Dirac cone can reproduce phenomena observed experimentally [27], such as the double-peak structure of the PHE, the sign change of the AMR, and unequal oscillating amplitudes between the AMR and PHE, with no need to introduce extra physics mechanisms. At the same time, since the nonlinear momentum terms universally exist in topological materials with spin-orbit interactions, it is expected that this tilt-induced PHE provides an alternative perspective to understand the nontopological origin of the PHE in TIs or even in Weyl/Dirac semimetals. We notice that the PHE reported in a recent experiment on type-II Dirac semimetals $NiTe_2$ [49] cannot be ascribed to the chiral anomaly or nontrivial Berry curvature but to an unknown nontopological origin. From Eq. (6), one can find that the appearance of off-diagonal components Σ_x and Σ_y introduces a B-dependent conductivity to pristine B^2-dependent conductivity in Eqs. (4), which provides a probability to exhibit B^β-dependent conductivity with fractional β as in Ref. [49].

Acknowledgments. This work was supported by GDUPS (2017), by National Natural Science Foundation of China (Grants No. 11874016 and No. 11904107), and by Key Program for Guangdong NSF of China (Grant No. 2017B030311003).

S.-H.Z. and H.-J.D. contributed equally to this work.

[1] J. Xiong, S. K. Kushwaha, T. Liang, J. W. Krizan, M. Hirschberger, W. Wang, R. J. Cava, and N. P. Ong, Science **350**, 413 (2015).

[2] C.-Z. Li, L.-X. Wang, H. Liu, J. Wang, Z.-M. Liao, and D.-P. Yu, Nat. Commun. **6**, 10137 (2015).

[3] H. Li, H. He, H.-Z. Lu, H. Zhang, H. Liu, R. Ma, Z. Fan, S.-Q. Shen, and J. Wang, Nat. Commun. **7**, 10301 (2016).

[4] T. Liang, J. Lin, Q. Gibson, S. Kushwaha, M. Liu, W. Wang, H. Xiong, J. A. Sobota, M. Hashimoto, P. S. Kirchmann, Z.-X. Shen, R. J. Cava, and N. P. Ong, Nat. Phys. **14**, 451 (2018).

[5] M. Hirschberger, S. Kushwaha, Z. Wang, Q. Gibson, S. Liang, C. A. Belvin, B. A. Bernevig, R. J. Cava, and N. P. Ong, Nat. Mater. **15**, 1161 (2016).

[6] X. C. Huang, L. X. Zhao, Y. J. Long, P. P. Wang, D. Chen, Z. H. Yang, H. Liang, M. Q. Xue, H. M. Weng, Z. Fang, X. Dai, and G. F. Chen, Phys. Rev. X **5**, 031023 (2015).

[7] C.-L. Zhang, S.-Y. Xu, I. Belopolski, Z. Yuan, Z. Lin, B. Tong, G. Bian, N. Alidoust, C.-C. Lee, S.-M. Huang, T.-R. Chang, G. Chang, C.-H. Hsu, H.-T. Jeng, M. Neupane, D. S. Sanchez, H. Zheng, J. Wang, H. Lin, C. Zhang, H.-Z. Lu, S.-Q. Shen, T. Neupert, M. Z. Hasan, and S. Jia, Nat. Commun. **7**, 10735 (2016).

[8] A. A. Burkov, Phys. Rev. B **91**, 245157 (2015).

[9] Xiao-Shi Li, Chen Wang, Ming-Xun Deng, Hou-Jian Duan, Pei-Hao Fu, Rui-Qiang Wang, L. Sheng, and D. Y. Xing, Phys. Rev. Lett. **123**, 206601 (2019).

[10] M.-X. Deng, G. Y. Qi, R. Ma, R. Shen, R. Q. Wang, L. Sheng, and D. Y. Xing, Phys. Rev. Lett. **122**, 036601 (2019).

[11] S. Zhong, J. Orenstein, and J. E. Moore, Phys. Rev. Lett. **115**, 117403 (2015).

[12] O. Breunig, Z. Wang, A. A. Taskin, J. Lux, A. Rosch, and Yoichi Ando, Nat. Commun. **8**, 15545 (2017).

[13] B. A. Assaf, T. Phuphachong, E. Kampert, V. V. Volobuev, P. S. Mandal, J. Sánchez-Barriga, O. Rader, G. Bauer, G. Springholz, L. A. de Vaulchier, and Y. Guldner, Phys. Rev. Lett. **119**, 106602 (2017).

[14] X. Dai, Z. Z. Du, and H.-Z. Lu, Phys. Rev. Lett. **119**, 166601 (2017).

[15] A. V. Andreev and B. Z. Spivak, Phys. Rev. Lett. **120**, 026601 (2018).

[16] A. A. Burkov, Phys. Rev. B **96**, 041110(R) (2017).

[17] S. Nandy, G. Sharma, A. Taraphder, and S. Tewari, Phys. Rev. Lett. **119**, 176804 (2017).

[18] Ming-Xun Deng, Hou-Jian Duan, Wei Luo, W. Y. Deng, Rui-Qiang Wang, and L. Sheng, Phys. Rev. B **99**, 165146 (2019).

[19] M. Wu, G. Zheng, W. Chu, Y. Liu, W. Gao, H. Zhang, J. Lu, Y. Han, J. Zhou, W. Ning, and M. Tian, Phys. Rev. B **98**, 161110(R) (2018).

[20] P. Li, C. H. Zhang, J. W. Zhang, Y. Wen, and X. X. Zhang, Phys. Rev. B **98**, 121108(R) (2018).

[21] R. Singha, S. Roy, A. Pariari, B. Satpati, and P. Mandal, Phys. Rev. B **98**, 081103(R) (2018).

[22] N. Kumar, S. N. Guin, C. Felser, and C. Shekhar, Phys. Rev. B **98**, 041103(R) (2018).

[23] H. Li, H.-W. Wang, H. He, J. Wang, and S.-Q. Shen, Phys. Rev. B **97**, 201110(R) (2018).

[24] H. X. Tang, R. K. Kawakami, D. D. Awschalom, and M. L. Roukes, Phys. Rev. Lett. **90**, 107201 (2003).

[25] K. M. Seemann, F. Freimuth, H. Zhang, S. Blügel, Y. Mokrousov, D. E. Bürgler, and C. M. Schneider, Phys. Rev. Lett. **107**, 086603 (2011).
[26] M. Bowen, K.-J. Friedland, J. Herfort, H.-P. Schönherr, and K. H. Ploog, Phys. Rev. B **71**, 172401 (2005).
[27] A. A. Taskin, H. F. Legg, F. Yang, S. Sasaki, Y. Kanai, K. Matsumoto, A. Rosch, and Y. Ando, Nat. Commun. **8**, 1340 (2017).
[28] B. Wu, X.-C. Pan, W. Wu, F. Fei, B. Chen, Q. Liu, H. Bu, L. Cao, F. Song, and B. Wang, Appl. Phys. Lett. **113**, 011902 (2018).
[29] D. Rakhmilevich, F. Wang, W. Zhao, M. H. W. Chan, J. S. Moodera, C. Liu, and C.-Z. Chang, Phys. Rev. B **98**, 094404 (2018).
[30] T. Chiba, S. Takahashi, and G. E. W. Bauer, Phys. Rev. B **95**, 094428 (2017).
[31] M. Trushin, K. Výborný, P. Moraczewski, A. A. Kovalev, J. Schliemann, and T. Jungwirth, Phys. Rev. B **80**, 134405 (2009).
[32] A. Sulaev, M. Zeng, S. Q. Shen, S. K. Cho, W. G. Zhu, Y. P. Feng, S. V. Eremeev, Y. Kawazoe, L. Shen, and L. Wang, Nano Lett. **15**, 2061 (2015).
[33] R. S. Akzyanov and A. L. Rakhmanov, Phys. Rev. B **97**, 075421 (2018).
[34] S. Nandy, A. Taraphder, and S. Tewari, Sci. Rep. **8**, 14983 (2018).
[35] S.-Q. Shen, *Topological Insulators: Dirac Equation in Condensed Matters* (Springer, Berlin, 2012).
[36] C.-X. Liu, X.-L. Qi, H. J. Zhang, X. Dai, Z. Fang, and S.-C. Zhang, Phys. Rev. B **82**, 045122 (2010).
[37] C. J. Tabert and J. P. Carbotte, Phys. Rev. B **91**, 235405 (2015).
[38] J.-H. Sun, L.-J. Wang, X.-T. Hu, L. Li, and D.-H. Xu, Phys. Rev. B **97**, 035130 (2018).
[39] C.-K. Chiu, Y.-H. Chan, X. Li, Y. Nohara, and A. P. Schnyder, Phys. Rev. B **95**, 035151 (2017).
[40] N. A. Sinitsyn, J. E. Hill, H. Min, J. Sinova, and A. H. MacDonald, Phys. Rev. Lett. **97**, 106804 (2006).
[41] N. A. Sinitsyn, A. H. MacDonald, T. Jungwirth, V. K. Dugaev, and J. Sinova, Phys. Rev. B **75**, 045315 (2007).
[42] M.-X. Deng, W. Luo, W. Y. Deng, M. N. Chen, L. Sheng, and D. Y. Xing, Phys. Rev. B **94**, 235116 (2016).
[43] See Supplemental Material at http://link.aps.org/supplemental/10.1103/PhysRevB.101.041408 for details of the derivations.
[44] A. M. Black-Schaffer, A. V. Balatsky, and J. Fransson, Phys. Rev. B **91**, 201411(R) (2015).
[45] A. V. Balatsky, I. Vekhter, and J. X. Zhu, Rev. Mod. Phys. **78**, 373 (2006).
[46] R. Q. Wang, L. Sheng, M. Yang, B. G. Wang, and D. Y. Xing, Phys. Rev. B **91**, 245409 (2015).
[47] Y. H. Xu, J. Chiu, L. Miao, H. W. He, Z. Alpichshev, A. Kapitulnik, R. R. Biswas, and L. Andrew Wray, Nat. Commun. **8**, 14081 (2017).
[48] H. Zhang, C.-X. Liu, X.-L. Qi, X. Dai, Z. Fang, and S.-C. Zhang, Nat. Phys. **5**, 438 (2009).
[49] Q. Q. Liu, F. C. Fei, B. Chen, X. Y. Bo, B. Y. Wei, S. Zhang, M. H. Zhang, F. J. Xie, M. Naveed, X. G. Wan, F. Q. Song, and B. G. Wang, Phys. Rev. B **99**, 155119 (2019).